

## Terahertz intersubband absorption in Ge/SiGe parabolic quantum wells

Michele Montanari,<sup>1</sup> Chiara Ciano,<sup>1</sup> Luca Persichetti,<sup>1</sup> Cedric Corley,<sup>2</sup> Leonetta Baldassarre,<sup>3</sup> Michele Ortolani,<sup>3</sup> Luciana Di Gaspare,<sup>1</sup> Giovanni Capellini,<sup>1,2</sup> David Stark,<sup>4</sup> Giacomo Scalari,<sup>4</sup> Michele Virgilio,<sup>5</sup> and Monica De Seta<sup>1</sup>

<sup>1</sup>*Dipartimento di Scienze, Università degli Studi Roma Tre, V.le G. Marconi 446, I-00146 Rome, Italy*

<sup>2</sup>*IHP-Leibniz-Institut für Innovative Mikroelektronik, Im Technologiepark 25, D-15236 Frankfurt (Oder), Germany*

<sup>3</sup>*Dipartimento di Fisica, Università di Roma “La Sapienza”, Piazzale A. Moro 2, I-00185 Rome, Italy*

<sup>4</sup>*Institute for Quantum Electronics, Department of Physics, ETH Zürich, Wolfgang-Pauli-Strasse 16, 8093 Zürich, Switzerland*

<sup>5</sup>*Dipartimento di Fisica “E. Fermi”, Università di Pisa, Largo Pontecorvo 3, I-56127 Pisa, Italy*

We demonstrate the deposition of high-quality, continuously graded Ge-rich  $\text{Si}_{1-x}\text{Ge}_x$  parabolic quantum wells with different doping level and geometry, on a Si substrate by ultrahigh vacuum chemical vapor deposition. A thorough structural characterization evidences the perfect parabolic compositional profile. THz absorption data, supported by theoretical calculations, showed for modulation doped samples a single optical resonance at constant energy up to 300 K. Following the Kohn’s theorem, this behavior is driven by the bare harmonic potential and is independent of temperature-induced variations of electron distribution.

Intersubband transitions (ISBTs) in semiconductor quantum wells (QWs) have been the focus of intense research in the last decades due to their importance for optoelectronic devices, such as quantum cascade lasers and quantum well photodetectors, and the rich physics that can be investigated, like the strong and ultrastrong light-matter coupling. In this context, parabolic quantum wells (PQWs) have been recently identified as a particularly interesting quantum system for THz applications in different fields, ranging from biology, medicine, security communications [add ref]. The main key feature of ISBTs in PQWs is that, according to the generalized Kohn’s theorem<sup>1,2</sup>, their energy is independent of the density and distribution of electrons in the QW. As a consequence, the performances of light emitters based on PQWs are expected to be unaffected by the temperature-induced variation of electron distribution. This is extremely relevant in terahertz optoelectronics where thermal charge fluctuations play a key role [add REF]. Furthermore, the equally spaced energy spectrum of PQWs made it possible to observe strong coupling in the THz range up to room temperature<sup>3</sup>.

Most of the PQWs structures investigated have been realized in III-V material systems<sup>3–9</sup> by exploiting molecular beam epitaxy (MBE). Despite the growth of III-V rectangular QWs by MBE is very well developed, the deposition of high-quality graded PQWs has been shown to be quite more challenging. Hence, many works<sup>3,4,7,8</sup> exploited the digital alloy technique, which consists in alternating layers of different composition to create an effective parabolic potential for the carriers. As a main drawback, the resulting structure shows a large number of interfaces, which are the source of undesirable scatterings. For CMOS-compatible  $\text{Si}_{1-x}\text{Ge}_x$  heterostructures grown on Si (001) substrates, which are more appealing for industrial applications, additional complexity to the

growth arises from the 4.2% lattice mismatch between Ge and Si<sup>10</sup>. The achievement of a parabolic profile is also complicated by surface segregation of Ge and Si-Ge intermixing occurring during the growth<sup>11</sup>.

In this Letter, we demonstrate the deposition of a stack of identical *n*-doped, continuously graded Ge-rich  $\text{Si}_{1-x}\text{Ge}_x$  PQWs. By exploring samples with different doping level and doping geometry, we investigate ISBT absorption spectra as a function of temperature, within the range from 10 K up to 300 K. Supported by theoretical calculations, we identify the doping approach in which electron-electron interactions cancel out leaving the optical resonance almost entirely governed by the bare parabolic potential.

The PQWs samples have been grown by ultrahigh-vacuum chemical vapor deposition (UHV-CVD) on Si (001) substrates by using ultrapure silane ( $\text{SiH}_4$ ) and germane ( $\text{GeH}_4$ ) without carrier gas. The sample growth started with a Si buffer layer, deposited at 850 °C, to restore a good surface quality after the substrate cleaning, performed with an *ex situ* wet-chemical cleaning followed by flash-heating to 1150 °C in hydrogen atmosphere to remove the native oxide. To achieve SiGe layers with high Ge concentration and low threading dislocation densities (about  $3.5 \times 10^6 \text{ cm}^{-2}$ [cite]), the PQWs have been deposited on top of a SiGe reverse-graded virtual substrate (VS)[add ref] with a final  $\text{Si}_{0.09}\text{Ge}_{0.91}$  alloy layer (see Fig. 1 (a)) following the procedure reported in Ref. 12[add montalenti]. The parabolic compositional profile with *x* in the 0.8 – 1 range is obtained by keeping the  $\text{GeH}_4$  gas flow constant and gradually varying the  $\text{SiH}_4$  flow by means of calibrated mass flow controllers. The module, composed by the parabolic well and a  $\text{Si}_{0.20}\text{Ge}_{0.80}$  barrier, has been repeated 20 times. The samples investigated were *n*-doped by phosphine co-deposition in the center of the parabolic well (direct

TABLE I. Sample parameters. The labelling is defined as M (D) for modulation (direct) doping - HD (LD) for high (low) doping.

Sample	Doping geometry	$n_{2D}$ (cm <sup>-2</sup> )
D-LD	Direct	$1.5 \times 10^{11}$
M-HD	Modulation	$3.5 \times 10^{11}$
D-HD	Direct	$6.0 \times 10^{11}$

doping, samples D-LD, D-HD) or in the center of the Si<sub>0.20</sub>Ge<sub>0.80</sub> barrier (modulation doping, sample M-HD) leaving an undoped Si<sub>0.20</sub>Ge<sub>0.80</sub> layer between the dopants and the well to reduce ionized impurity scattering<sup>13</sup>. The donor density has been calibrated by secondary ion mass spectrometry (SIMS, not reported here) and the actual sheet-carrier density  $n_{2D}$  was directly measured by Fourier Transform Infrared (FTIR) spectroscopy. The samples were characterized by using high resolution x-ray diffraction (HR-XRD), SIMS, scanning transmission electron microscopy (STEM), and FTIR spectroscopy. Specific information on individual samples can be found in Table I.

The compositional profile across the PQWs has been accurately evaluated by SIMS. The results reported in Fig. 1 (b-c) show that the profile of the Ge composition perfectly matches a parabola.

HR-XRD measurements were carried out with a SmartLab diffractometer from Rigaku using CuK $\alpha$  radiation, a Ge (400)  $\times$  2 beam collimator and a Ge (220)  $\times$  2 analyzer crystal. The positions of the VS spots associated to the Ge and the Si<sub>0.09</sub>Ge<sub>0.91</sub> layers in the HR-XRD reciprocal space maps around asymmetric (4 $\bar{2}\bar{2}$ ) reflections reported in Fig. 1 (e) reveal, at room temperature, a tensile strain of about +0.2%, which can be ascribed to the difference between the coefficients of thermal expansion in Ge and Si<sup>14,15</sup>. Thus, the in-plane lattice parameter of the Si<sub>0.09</sub>Ge<sub>0.91</sub> layer is equivalent, at room temperature, to the lattice parameter of a Si<sub>0.05</sub>Ge<sub>0.95</sub> relaxed bulk alloy, being, therefore, tensile strained in the growth plane with  $\varepsilon_{\parallel} = 0.17\%$ . Together with the reflections due to the Ge and the Si<sub>0.09</sub>Ge<sub>0.91</sub> layers, we observe multiple orders of superlattice (SL) satellites which are perfectly vertically aligned to the Si<sub>0.09</sub>Ge<sub>0.91</sub> buffer, indicating that the entire PQW stack is coherent with the in-plane lattice parameter of the underlying VS. Figure 1(d) shows the XRD rocking curve around the (004) Ge and (004) Si Bragg peaks together with the result of the simulation software ‘‘MadMax’’. In the XRD simulation, the parabolic fit of the SIMS data, reported in Fig. 1(b), has been used as input compositional profile. The high quality-factor of the SL fringes (indicated by the red arrows in Fig. 1 (d)) confirms the high crystalline quality and the regular periodicity of the PQWs in the stack. Moreover, the

good agreement between XRD data and simulations confirms the parabolic symmetry of the compositional profile.

The electronic band structure and ISBT energies of the investigated samples have been calculated self-consistently, relying on a well-established and extensively tested multivalley effective mass Schrödinger-Poisson solver<sup>16–19</sup>. A detailed description of the model can be found in Ref. 20; here, we only mention that contributions to the Hartree potential from electrons at the  $\Gamma$ ,  $\Delta$ , and  $L$  valleys, and exchange-correlations effects in the local density approximation are fully taken into account.

A parabolic well of width  $W$  and height  $\Delta_0$  has an oscillator energy<sup>21</sup>  $E_0 = \hbar\omega_0 = \hbar(8\Delta_0/W^2m_z^*)^{1/2}$ , where  $m_z^*$  is the effective mass in the growth direction. Thus, in our samples, where  $W \sim 48 - 50$  nm,  $\Delta_0 \sim 120$  meV and  $m_z^* = 0.135 m_0$ <sup>17</sup>, the bare oscillator energy is  $E_0 \sim 15.3$  meV. However, the self-consistent confining potential is affected by the presence of both ionized donor P atoms and by electron charge distribution. Taking these effects into account, we show, in Fig. 2, the  $L$  band-edge profile and the squared wavefunctions, self-consistently calculated for samples in Table I. By comparing the left and right panels of Fig. 2, i.e. direct and modulation doping, we note that electrostatic (Hartree) charge effects affects the  $L$  band profile in a different way for the two different doping geometries. As a matter of fact, when donors are introduced directly in the well, the bottom of the parabola visually deepens (the effective confining height  $\Delta_{eff}$  increases,  $\Delta_{eff} > \Delta_0$ ) and, for high doping, the parabolic potential is lost; consequently, the subband energies are no more equally spaced but low energies states have a larger energy separation with respect to the bare value ( $E_{12} > \hbar\omega_0$ ). On the contrary, in the case of modulation doping,  $\Delta_{eff}$  decreases ( $\Delta_{eff} < \Delta_0$ ). Therefore, in the case of direct doping, the Hartree potential is expected to blueshift the absorption resonance while, for the modulation doping approach, to redshift it. This is consistent with the fact that only in modulation-doped samples the depolarization blueshift can compensate for the Hartree potential, regardless of the electron density and its distribution in the subbands [add ref], and, thus, the Kohn theorem holds [add REF].

Having discussed the electronic ISB features of our PQW samples, we now show absorption measurements performed between 10 and 300 K to investigate the dependence of the absorption resonance on doping and temperature. Absorption spectra were measured as a function of temperature in side-illuminated single-pass waveguide configuration with a FTIR spectrometer (Bruker Vertex 70v), equipped with a He-flow cryostat. The samples were cut and polished in a prism-waveguide geometry to couple the incoming radiation to the ISB dipole

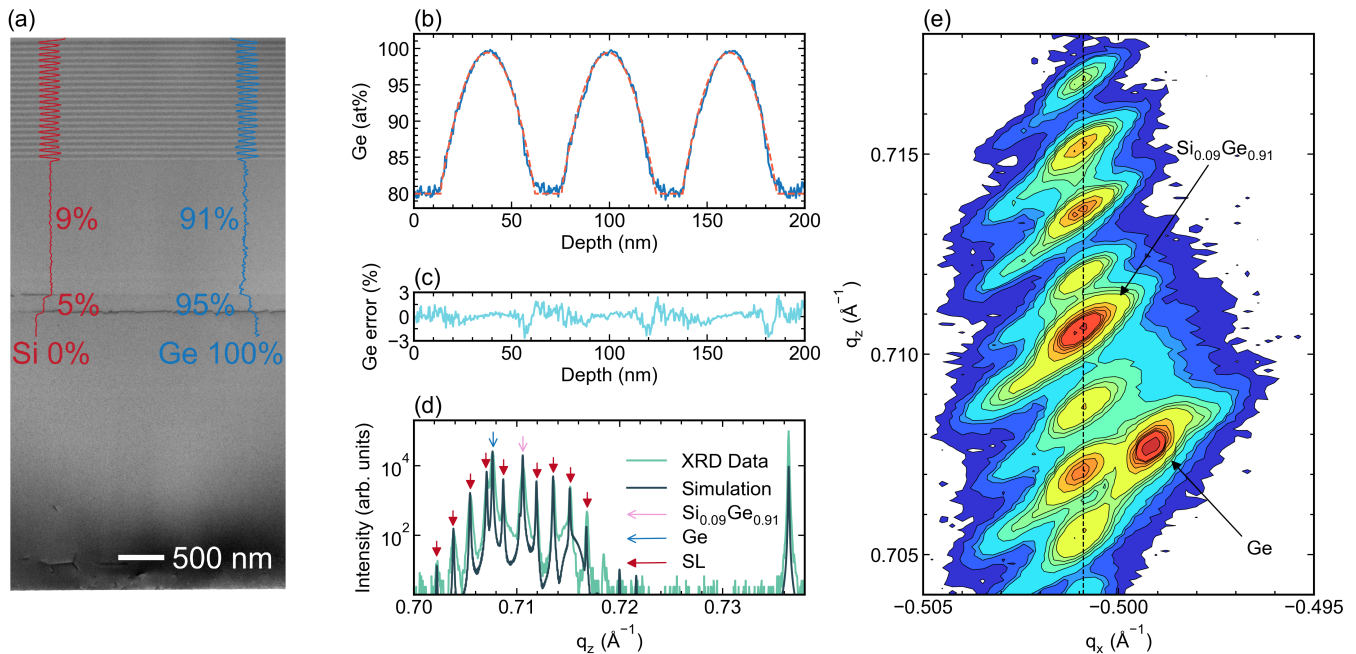


FIG. 1. (Color online) (a) Secondary-ion mass spectrometry (SIMS) composition profile of a PQW sample superimposed on its STEM image. (b) Enlarged view of the SIMS composition profile (blue curve) and parabolic fit (orange curve). Panel (c) shows the difference between the two curves in (b). (d) (004) XRD rocking curve and (e) reciprocal space map of asymmetric ( $4\bar{2}2$ ) reflections, respectively.

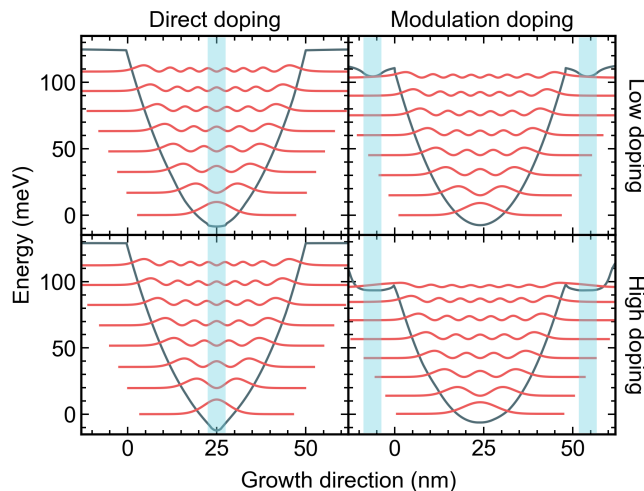


FIG. 2. (Color online) Electron energy and squared wave-functions for the samples investigated. Gray curves represent the  $L$  band profiles. The doped region in both the samples is indicated by the light blue shadows.

moment (i.e., TM polarized)<sup>22,23</sup>. The dichroic transmittance  $T(E)$ , shown in Fig. 3, is obtained as the ratio between the transmitted beam intensity in the TM and in the TE polarization. The dips at  $\simeq 18$  (4.3),  $\simeq 30$  (7.2), and  $\simeq 19$  (4.8) meV (THz) are the signatures of the intersubband transition  $E_{12}$  in samples D-LD, D-HD, and M-HD, respectively. The FWHM is 6.4, 19.3,

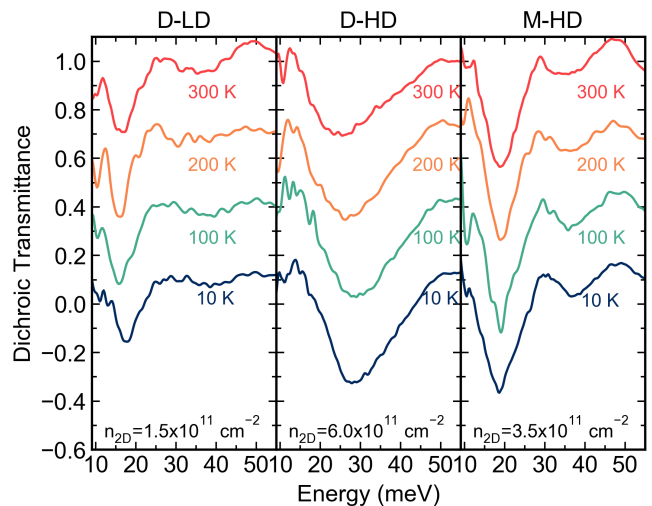


FIG. 3. (Color online) TM to TE waveguide mode transmittance ratio for three samples at increasing doping concentrations at  $T=10, 100, 200,$  and  $300$  K. Dips at  $\simeq 18$  (sample D-LD),  $\simeq 30$  meV (sample D-HD), and  $\simeq 20$  (sample M-HD) are the signature of the intersubband transition. Spectra are vertically offset in steps of 0.3 for clarity.

and 11.0 meV respectively, in agreement with previous reports for square QWs with similar doping profiles [add REF]. Interestingly, in sample D-LD and in sample M-HD, the peak energy and width are almost independent of

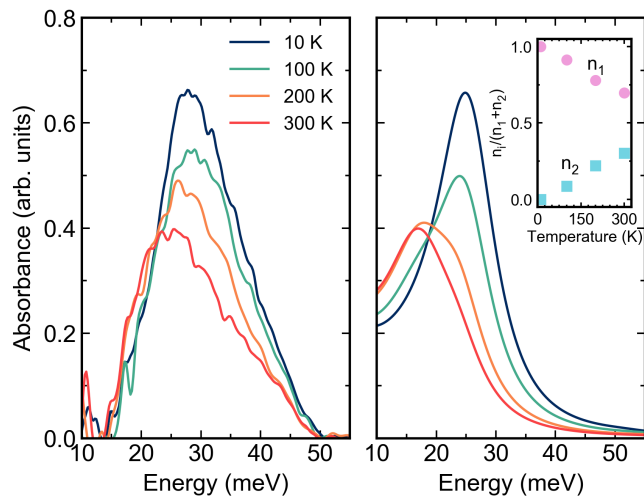


FIG. 4. (Color online) Measured (left panel) and calculated (right panel) 2D absorbance spectra acquired on sample D-HD at different  $T$ .

temperature and close to the theoretical bare value  $\hbar\omega_0$ , despite the fact that several subbands are occupied at room temperature: our calculations indicate that  $\sim 42\%$  of electrons are in subband 1,  $\sim 25\%$  are in subband 2, and  $\sim 14\%$  in subband 3. A different behavior was observed in sample D-HD, where the ISB absorption redshifts at increasing temperature. Furthermore, the transmittance dip broadens, and becomes asymmetric at high temperature, suggesting that the contribute of different transitions is present<sup>24</sup>. In order to confirm this hypothesis, in Fig. 4, we compared the measured 2D absorbance  $\alpha_{2D}$  of D-HD with its theoretical absorption spectrum. The simulation shows that the energy separation between the ground and the first-excited subband in this sample is 19.6 meV and that a significant fraction of electrons occupy the first-excited subband at 300 K, as shown in the inset of the figure. Therefore, the contribution to the absorption of the  $E_{23}$  transition is dominant at room temperature. The  $2 \rightarrow 3$  absorption resonance occurs at lower energy with respect to the  $1 \rightarrow 2$  absorption at 10 K because of the smaller  $E_{23}$  energy separation and the negligible [or lower?] depolarization shift. Our findings indicate that, to achieve a temperature independent absorption in direct doped PQWs, the electron density must be  $\sim 1 \times 10^{11}$ , as in sample D-LD, so that the Hartree potential and the depolarization shift are almost negligible.

The most interesting feature of our absorption experiment is that, in modulation doped samples, the absorption spectrum is independent of both temperature and subband occupation, also at high doping (sample M-HD). As already observed, this feature is related to the presence of electron correlation effects and to the validity of the generalized Kohn theorem for the modulation doping geometry, in which the impurity charges are far from the parabolic potential well. The observed behavior

can also be derived in the framework of the dipole gauge Hamiltonian, considering the collective “multisubband” plasmon modes that arise from the interaction between different ISB transitions<sup>9</sup>. In this framework, it was shown that the ISB absorption strength in PQWs is concentrated in a single mode at the frequency of the bare ISB transition of the undoped well regardless of doping and temperature, consistently with what we also observe.

Recently<sup>6</sup>, THz IBSTs in  $\text{Al}_x\text{Ga}_{1-x}\text{As}$  PQWs have been investigated as a function of temperature. As in our case, the absorption energy was found to be independent of temperature, while a broadening of the absorption peak was observed at increasing temperature. For a sheet density  $n_{2D} = 3 \times 10^{11} \text{ cm}^{-2}$ , thus slightly smaller than in sample M-HD, the authors reported that  $\Delta E/E$  raised from 12% to 30% when the temperature was increased from 77 K to room temperature. In sample M-HD we found  $\Delta E/E \sim 35\%$ , independent of temperature. Thus, at room temperature, the  $\Delta E/E$  values are comparable for the two material systems.

In conclusion, we have demonstrated the growth of high-quality, continuously graded  $\text{Si}_{1-x}\text{Ge}_x$  PQWs by UHV-CVD. In modulation doped samples, we observe a single ISB absorption peak whose energy position and shape do not change from 10 K up to room temperature, also for high doping levels. These achievements represent a relevant step forward toward the development of THz devices based on PQWs and compatible with the CMOS technology.

## ACKNOWLEDGMENTS

This work is supported by the European Union research and innovation programme Horizon 2020 under grant No. 766719 - FLASH Project.

- <sup>1</sup>W. Kohn, Phys. Rev. **123**, 1242 (1961).
- <sup>2</sup>L. Brey, N. F. Johnson, and B. I. Halperin, Phys. Rev. B **40**, 10647 (1989).
- <sup>3</sup>M. Geiser, G. Scalari, F. Castellano, M. Beck, and J. Faist, Applied Physics Letters **101**, 141118 (2012), <https://doi.org/10.1063/1.4757611>.
- <sup>4</sup>K. D. Maranowski and A. C. Gossard, Journal of Applied Physics **88**, 172 (2000), <https://doi.org/10.1063/1.373638>.
- <sup>5</sup>C. Deimert and Z. Wasilewski, Journal of Crystal Growth **514**, 103 (2019).
- <sup>6</sup>C. Deimert, P. Goulain, J.-M. Manceau, W. Pasek, T. Yoon, A. Bousseksou, N. Y. Kim, R. Colombelli, and Z. R. Wasilewski, Phys. Rev. Lett. **125**, 097403 (2020).
- <sup>7</sup>R. C. Miller, A. C. Gossard, D. A. Kleinman, and O. Munteanu, Phys. Rev. B **29**, 3740 (1984).
- <sup>8</sup>J. Ulrich, R. Zobl, K. Unterrainer, G. Strasser, E. Gornik, K. D. Maranowski, and A. C. Gossard, Applied Physics Letters **74**, 3158 (1999), <https://doi.org/10.1063/1.124091>.
- <sup>9</sup>A. Delteil, A. Vasanelli, Y. Todorov, C. Feuillet Palma, M. Renaudat St-Jean, G. Beaudoin, I. Sagnes, and C. Sirtori, Phys. Rev. Lett. **109**, 246808 (2012).
- <sup>10</sup>G. Capellini, M. De Seta, Y. Busby, M. Pea, F. Evangelisti, G. Nicotra, C. Spinella, M. Nardone, and

- C. Ferrari, *Journal of Applied Physics* **107**, 063504 (2010), <https://doi.org/10.1063/1.3327435>.
- <sup>11</sup>A. Ballabio, J. Frigerio, S. Firoozabadi, D. Chrastina, A. Beyer, K. Volz, and G. Isella, *Journal of Physics D: Applied Physics* **52**, 415105 (2019).
- <sup>12</sup>O. Skibitzki, M. H. Zoellner, F. Rovaris, M. A. Schubert, Y. Yamamoto, L. Persichetti, L. Di Gaspare, M. De Seta, R. Gatti, F. Montalenti, and G. Capellini, *Phys. Rev. Materials* **4**, 103403 (2020).
- <sup>13</sup>M. Virgilio, D. Sabbagh, M. Ortolani, L. Di Gaspare, G. Capellini, and M. De Seta, *Phys. Rev. B* **90**, 155420 (2014).
- <sup>14</sup>G. Capellini, M. De Seta, P. Zaumseil, G. Kozlowski, and T. Schroeder, *Journal of Applied Physics* **111**, 073518 (2012), <https://doi.org/10.1063/1.3702443>.
- <sup>15</sup>C. Manganelli, M. Virgilio, O. Skibitzki, M. Salvalaglio, D. Spirito, P. Zaumseil, Y. Yamamoto, M. Montanari, W. Klesse, and G. Capellini, *Journal of Raman Spectroscopy* **51**, 989 (2020), <https://onlinelibrary.wiley.com/doi/pdf/10.1002/jrs.5860>.
- <sup>16</sup>M. Montanari, M. Virgilio, C. L. Manganelli, P. Zaumseil, M. H. Zoellner, Y. Hou, M. A. Schubert, L. Persichetti, L. Di Gaspare, M. De Seta, E. Vitiello, E. Bonera, F. Pezzoli, and G. Capellini, *Phys. Rev. B* **98**, 195310 (2018).
- <sup>17</sup>C. Ciano, M. Virgilio, M. Montanari, L. Persichetti, L. Di Gaspare, M. Ortolani, L. Baldassarre, M. Zoellner, O. Skibitzki, G. Scalari, J. Faist, D. Paul, M. Scuderi, G. Nicotra, T. Grange, S. Birner, G. Capellini, and M. De Seta, *Phys. Rev. Applied* **11**, 014003 (2019).
- <sup>18</sup>L. Persichetti, M. Montanari, C. Ciano, L. Di Gaspare, M. Ortolani, L. Baldassarre, M. Zoellner, S. Mukherjee, O. Moutanabbir, G. Capellini, M. Virgilio, and M. De Seta, *Crystals* **10** (2020), 10.3390/cryst10030179.
- <sup>19</sup>C. Ciano, L. Persichetti, M. Montanari, L. Di Gaspare, G. Capellini, L. Baldassarre, M. Ortolani, A. Pashkin, M. Helm, S. Winnerl, M. Virgilio, and M. De Seta, *Phys. Rev. B* **102**, 205302 (2020).
- <sup>20</sup>L. Bagolini, M. Montanari, L. Persichetti, L. Di Gaspare, G. Capellini, M. Ortolani, M. De Seta, and M. Virgilio, *Phys. Rev. B* **101**, 245302 (2020).
- <sup>21</sup>K. D. Maranowski, A. C. Gossard, K. Unterrainer, and E. Gornik, *Applied Physics Letters* **69**, 3522 (1996), <https://doi.org/10.1063/1.117232>.
- <sup>22</sup>M. De Seta, G. Capellini, Y. Busby, F. Evangelisti, M. Ortolani, M. Virgilio, G. Grosso, G. Pizzi, A. Nucara, and S. Lupi, *Applied Physics Letters* **95**, 051918 (2009), <https://doi.org/10.1063/1.3198204>.
- <sup>23</sup>Y. Busby, M. De Seta, G. Capellini, F. Evangelisti, M. Ortolani, M. Virgilio, G. Grosso, G. Pizzi, P. Calvani, S. Lupi, M. Nardone, G. Nicotra, and C. Spinella, *Phys. Rev. B* **82**, 205317 (2010).
- <sup>24</sup>M. D. Seta, G. Capellini, M. Ortolani, M. Virgilio, G. Grosso, G. Nicotra, and P. Zaumseil, *Nanotechnology* **23**, 465708 (2012).